

Reconfigurable Intelligent Surface Optimal Placement in Millimeter-Wave Networks

Konstantinos Ntontin, *Member, IEEE*, Alexandros–Apostolos A. Boulogeorgos, *Senior Member, IEEE*,
Dimitrios Selimis, *Graduate Student Member, IEEE*, Fotis Lazarakis,
Angeliki Alexiou, *Member, IEEE*, and Symeon Chatzinotas, *Senior Member, IEEE*

This work discusses the optimal placement of a reconfigurable intelligent surface (RIS) in a millimeter wave (mmWave) point-to-point link. In particular, we present a novel system model that takes into account the relationship between the transmission beam footprint size at the RIS plane and the RIS size. Moreover, we present the theoretical framework that quantifies the RIS gain loss in the case that the transmission beam footprint in the RIS plane is smaller than the RIS size, and the beam waste for the case in which the transmission beam footprint in the RIS plane is larger than the RIS size, by extracting closed-form expressions for the received power and the end-to-end signal-to-noise-ratio (SNR) for both cases. Subsequently, building upon the expressions, we provide SNR maximization policies for both cases. Finally, we perform a comparison, in terms end-to-end SNR, between the RIS-aided link and its relay-aided counterpart.

Index Terms—Optimal placement, Reconfigurable intelligent surfaces, Relays, Signal-to-noise ratio analysis.

NOMENCLATURE

3D	Three-Dimensional
AF	Amplify-and-Forward
B5G	Beyond the Fifth Generation
DF	Decode-and-Forward
FD	Full-Duplex
HD	Half-Duplex
HPBW	Half-Power Beamwidth
LoS	Line-of-Sight
mmWave	Millimeter Wave
NLoS	Non-Line-of-Sight
PIN	Positive-Intrinsic-Negative
RF	Radio-Frequency
RIS	Reconfigurable Intelligent Surface
RU	Reflection Unit
RX	Receiver
SNR	Signal-to-Noise-Ratio
TX	Transmitter

I. INTRODUCTION

Increasing data-rate demands have led current mobile-access networks relying on sub-6 GHz bands reach their limits in

terms of available bandwidth. This bottleneck created the need to consider above-6 GHz bands for mobile-access networks. Currently, bands in the lower-end millimeter wave (mmWave) spectrum are used for point-to-point and point-to-multipoint line-of-sight (LoS) wireless backhaul/fronthaul and fixed-wireless access networks [1]. Such deployments span the 30-100 GHz operational frequency range. However, the expected migration of future mobile-access networks to the 30 – 100 GHz band pushes the corresponding wireless backhaul/fronthaul links towards the beyond-100 GHz bands. Due to this, backhauling/fronthauling transceiver equipment vendors have performed LoS trials in the D-band (130 – 174.8 GHz), which showcase the potential of using it in such deployments [2]. Apart from LoS, street-level deployments in dense urban scenarios necessitate devising non-LoS (NLoS) solutions since LoS links may not always be available. However, despite the fact that according to measurements [3], [4] NLoS communication through scattering and reflection from objects in the radio path is feasible in the 30 – 100 GHz range, the higher propagation loss of beyond-100 GHz bands is likely to challenge this assumption.

The conventional approach of counteracting NLoS links is by providing alternative LoS routes through relay nodes [5]. Although this is a well-established method to increase the coverage when the signal quality of the direct links is low, it is argued that it cannot constitute a viable approach for massive deployment, especially for mmWave networks. This is due to the increased power consumption of the active radio-frequency (RF) components in high frequencies that relays need to be equipped with [6]. Apart from relaying, communication through passive non-reconfigurable specular reflectors, such as dielectric mirrors, has been proposed as another alternative. Such a method for coverage enhancement has the potential to be notably more cost efficient compared with relaying and has been documented at both mmWave and beyond-100 GHz bands [6], [7]. Due to the highly dynamic nature of blockage at high frequencies together with the traffic conditions which may necessitate fast rerouting of information

K. Ntontin is with the Interdisciplinary Centre for Security, Reliability and Trust (SnT) – University of Luxembourg, L-1855 Luxembourg, and the Wireless Communications Laboratory of the Institute of Informatics and Telecommunications, National Centre for Scientific Research–“Demokritos,” Athens, Greece. E-mail: kostantinos.ntontin@uni.lu.

A.-A. A. Boulogeorgos and A. Alexiou are with the Department of Digital Systems, University of Piraeus Piraeus 18534 Greece. E-mails: al.boulogeorgos@ieee.org, alexiou@unipi.gr.

D. Selimis and F. Lazarakis are with the Wireless Communications Laboratory of the Institute of Informatics and Telecommunications, National Centre for Scientific Research–“Demokritos,” Athens, Greece. E-mails: {dselimis, flaz}@iit.demokritos.gr.

S. Chatzinotas is with the Interdisciplinary Centre for Security, Reliability and Trust (SnT) – University of Luxembourg, L-1855 Luxembourg. E-mail: symeon.chatzinotas@uni.lu.

This work was supported by the European Commission’s Horizon 2020 research and innovation programme (ARIADNE) under grant agreement No. 871464 and the Luxembourg National Research Fund (FNR) under the CORE project RISOTTI.

within a network, it would be desirable that such reflectors can change the angle of departure of the waves so that they direct the beams towards different routes. However, passive reflectors are incapable of supporting the aforementioned functionality since the conventional Snell's law applies. Furthermore, even by enabling this functionality by means of mechanical steering of the passive reflectors, the resulting latency would substantially compromise the desired reliability. Based on the above, an intriguing question that arises is the following: *Would it be possible to deploy reconfigurable reflectors that can arbitrarily steer the impinging beam based on dynamic blockage and traffic conditions and without compromising the desired latency?* The answer is affirmative by considering the reconfigurable intelligent surface (RIS) paradigm.

RISs are two-dimensional structures of dielectric material, which embed tunable reflection units (RUs) [8]–[12]. They constitute a substantially different technology than relaying, due to the absence of bulky and power-hungry analog electronic components, such as power amplifiers and low-noise amplifiers. Additionally, their operation, in contrast with relaying, does not require dividers and combiners, which can incur high insertion losses. By individually tuning the phase response of each individual RIS element, the reflected signals can constructively aggregate at a particular focal point, such as the receiver. Such a tuning can be enabled by electronic phase-switching components, such as positive-intrinsic-negative (PIN) diodes, RF-microelectromechanical systems, and varactor diodes, that are introduced between adjacent elements [13]. Hence, RISs offer an alternative-to-relaying method for large-scale beamforming without the incorporation of high power consuming electronics and insertion losses involved by the additional circuitry. In practice, the RIS element phase shift can be controlled by a central controller through programmable software [13].

Recognizing the unprecedented features that RISs can bring to beyond the fifth generation (B5G) wireless systems, a great amount of research effort has been put on analyzing, designing and optimizing RIS-aided wireless systems [13]–[17], as well as comparing them with their predecessors, i.e., relaying-aided ones [11], [18]–[20]. In more detail, in [13] and [14], the authors introduced the idea of employing RIS in order to mitigate the impact of blockage and steer the transmission beam towards the desired direction. Likewise, in [15], the authors presented the optimization framework for the maximization of the reception power in a RIS-aided system, assuming that all the RIS area can be used to reflect the induced electromagnetic wave. Moreover, in [16], the authors studied the asymptotic uplink ergodic capacity performance of a RIS-aided wireless system, while, in [17], the coverage of a downlink RIS-assisted network was studied, assuming that the entire RIS area can be used, and a strategy for maximizing the cell coverage by optimizing the RIS orientation and horizontal distance was proposed.

As far as the comparison with relays is concerned, in [11] the authors derive closed-form average signal-to-noise-ratio (SNR), outage probability, and symbol-error-rate expressions for a sub-6 GHz point-to-point RIS-aided link between a single-antenna source and destination and compare the

achievable performance with an amplify-and-forward (AF) relay. According to their findings, the RIS-based link outperforms its relay-based counterpart. In [18], the authors compare the achievable rate of RIS-aided systems with both the half-duplex (HD) and full-duplex (FD) relaying ones and show that a sufficiently large RIS is needed to guarantee the same rate performance with a single-antenna relay when the former is used for anomalous reflection instead of beamforming/focusing. [19] reveals that RIS-aided systems outperform the corresponding amplify-and-forward relaying ones for about 300% in terms of energy efficiency. Finally, contrary to the findings of [19], in [20] the authors show that an RIS needs hundred of radiating elements to outperform, in terms of rate, a single-antenna HD and decode-and-forward (DF) relay. In addition, they show that the RIS can be more energy efficient than the relay only for very high data rates.

Motivation, novelty, and contribution: All the presented RIS-related works consider the case of the entire RIS area being illuminated by the transmitted beam. However, due to the highly directional transmissions in mmWave networks and the low manufacturing cost of RISs, which make them suitable, as it is envisioned, to cover a big portion of the facades of large structures, such as buildings, it is expected that in many cases only a part of the total RIS area is going to be illuminated. Based on this, our work is motivated by the need to answer the question of what the optimal RIS placement policy is, which can be seen as a network planning question, in the two cases of the RIS area being smaller and larger than the transmitted beam footprint. Summarizing, the technical contribution of the paper is as follows:

- We present a system model for an RIS-aided mmWave links of fixed topology, such as wireless backhaul/fronthaul links, and use electromagnetic theory to evaluate the received power for the cases in which the transmission footprint at the RIS plane is smaller and larger than the RIS. The derived expressions, apart from the TX, RIS and RX positions, take into account the antenna characteristics as well as the RIS particularities, and quantify the performance degradation due to RIS underexploitation or beam waste. Of note, the presented analysis can also find application in mobile mmWave networks.
- Based on these expressions, we evaluate the end-to-end SNR for both cases in which the transmission beam footprint at the RIS plane is smaller and larger than the RIS. For the case in which the the transmission beam footprint at the RIS plane is larger than the RIS, we also define the beam waste and extract a simple closed-form expression for its evaluation.
- Subsequently, we analytically extract two policies for the optimum RIS placement for both cases under investigation.
- Finally, we compute the end-to-end SNR for a HD and DF relay-aided link and compare it with the corresponding RIS-aided one. The analytical results, which are verified by means of simulations, reveal a different monotonic behavior of the SNR ratio with respect to

the transmitter (TX)-receiver (RX) distance for small and large RIS structures.

Organization: The rest of this contribution is structured as follows: In Section II, the system model is presented, while, in Section III, we report the end-to-end SNR. Moreover, the optimal RIS placement problem is discussed and solved in Section IV, whereas, an insightful comparison against the corresponding relaying system is provided in Section V. Numerical results and discussions are given in Section VI. Finally, Section VII concludes the paper by highlighting the most important findings and remarks.

Notation: For the convenience of the readers, recurrent parameters and symbols with their meaning are presented in Table I.

TABLE I
RECURRENT PARAMETERS AND SYMBOLS.

Parameter/Symbol	Meaning
f	Carrier frequency
λ	Wavelength
P_t	Transmit power
W	Signal bandwidth
\mathcal{F}_{dB}	Noise figure
N_0	Thermal noise power
h_{RIS}/h_{rel}	RIS/relay height with respect to the ground
h_t/h_r	TX/RX height with respect to the ground
D_t/D_r	TX/RX/relay antenna diameter
ϕ_t/ϕ_r	TX/RX/relay antenna HPBW
e_t/e_r	TX/RX/relay antenna aperture efficiency
G_t/G_r	TX/RX/relay antenna gain
Γ	Amplitude reflection coefficient of the RUs
p	Parameter defining the steepness of the RU radiation pattern
γ	RU gain in the broadside direction
d_x, d_y	x-axis and y-axis length, respectively, of the RUs
α, β	Radii of the TX beam elliptic footprint
ϵ	Eccentricity of TX beam elliptic footprint
r_1	Distance between the center of the TX antenna and the center of the TX footprint at the RIS plane
r_2	Distance between the center of the TX footprint at the RIS plane and the center of the RX antenna
$r_{1,h}, r_{1,rel,h}$	TX-RIS and TX-relay horizontal distance
$r_{1,h}^*, r_{1,rel,h}^*$	Optimal RIS and relay, respectively, horizontal distance
r_h	TX-RX horizontal distance
θ_i, θ_r	Electromagnetic wave incidence and departure angles, respectively
S_{RIS}	RIS area
S_i	Area of the TX beam elliptic footprint
ϵ_w	Beam waste
P_r	Received power of the RIS-aided link
ρ_{RIS}	SNR of the RIS-aided link in the $S_{RIS} < S_i$ case
ρ_i	SNR of the RIS-aided link in the $S_{RIS} > S_i$ case
$\rho_{1,rel}^{(1)}$	SNR of the relay-aided link in the 1st hop
$\rho_{2,rel}^{(2)}$	SNR of the relay-aided link in the 2nd hop
$\rho_{rel}^{(DF)}$	SNR of the relay-aided link
$\zeta_{RIS,rel}$	Ratio of the optimal values of ρ_{RIS} and $\rho_{rel}^{(DF)}$
$\zeta_{i,rel}$	Ratio of the optimal values of ρ_i and $\rho_{rel}^{(DF)}$

II. SYSTEM MODEL

As illustrated in Fig. 1, we consider a fixed-topology scenario, in which a TX communicates with a RX through an RIS. θ_i and θ_r are the incidence and departure angles, respectively, of the electromagnetic wave. The TX-RIS and RIS-RX LoS links are established in a mmWave band and constitute an alternative path to the direct TX-RX link that is assumed to be blocked. To countermeasure the high pathloss in this band, both the TX and RX are equipped with highly directional

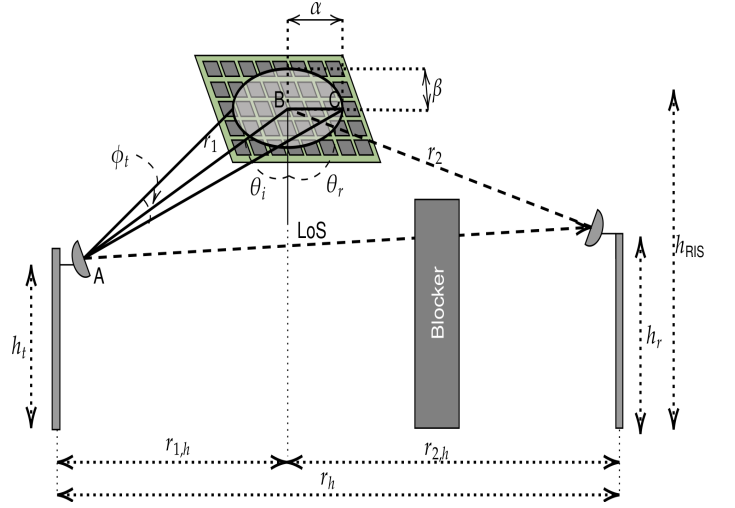


Fig. 1. System model.

parabolic antennas with diameters D_t and D_r , respectively. As a result, their gains can be obtained as [21]

$$G_m = e_m \left(\frac{\pi D_m}{\lambda} \right)^2, \text{ with } m \in \{t, r\}, \quad (1)$$

where e_t and e_r respectively denote the aperture efficiencies of the TX and RX parabolic reflectors, while λ represents the transmission wavelength. Note that this type of antennas has been extensively used for wireless backhaul/fronthaul scenarios (see e.g., [22] and reference therein), due to their capability to support pencil-beamforming transmissions. Under such directional transmissions, almost the entire transmit energy is located within the half-power beamwidth (HPBW) [6] and the three-dimensional (3D) antenna pattern can be modeled as a cone for HPBWs smaller than approximately 15° [23, Ch. 12]. The HPBW of the TX and RX antennas can be tightly approximated as in [24]

$$\phi_m \approx \frac{1.22\lambda}{D_m}, \text{ with } m \in \{t, r\}. \quad (2)$$

By substituting (2) into (1), we can rewrite the TX and RX antenna gains as

$$G_m \approx \left(\frac{1.22\pi}{\phi_m} \right)^2 e_m, \text{ with } m \in \{t, r\}. \quad (3)$$

Likewise, we assume that the TX and RX antennas can be mechanically steered, both in azimuth and elevation, towards the desired angle of transmission and reception, respectively, and they are pointing towards the center of illuminated RIS region.

The RIS acts as a beamformer, which by adjusting the phase response of the RUs is capable of steering the beam at θ_r , which is the RX direction. It consists of $N_x \times N_y$ RUs of size $d_x \times d_y$ and a controller that has perfect knowledge of the TX and RX positions. Each RU is an electrically-small low-gain element embedded on a substrate, with radiation pattern that can be expressed as in [25]

$$G_{RIS}(\theta) = \gamma \cos^p(\theta), \text{ with } 0 \leq \theta < \pi/2, \quad (4)$$

where γ stands for the RU gain and p is a constant that determines the steepness of the radiation pattern and depends on the RU type. Based on [25], γ can be evaluated as

$$\gamma = 2(2p + 1). \quad (5)$$

Due to the the fact that the TX-RIS and RIS-RX links are directional LoS links, they are deterministic. Moreover, it is assumed that the transmission power is P_t and that the received signal is subject to additive white Gaussian noise with power

$$N_0 = -174 + 10 \log_{10}(W) + \mathcal{F}_{\text{dB}}, \quad (6)$$

where \mathcal{F}_{dB} is the noise figure in dB and W is the transmission bandwidth [26].

III. SNR

In this section, we firstly derive the illuminated RIS area and, subsequently, compute the resulting end-to-end SNR in the two cases of the RIS area being smaller and larger than the transmitted beam footprint.

A. RIS's Illuminated Area

Since the main lobe of the transmission antenna has a conical shape, its footprint in the RIS plane is an ellipse, according to the conic-section theory [27]. The following Lemma returns the two radii of the illuminated elliptic area at the RIS.

Lemma 1: The two radii of the illuminated elliptic area at the RIS plane can be obtained as

$$\alpha = \frac{\sin\left(\frac{\phi_t}{2}\right)}{\cos\left(\theta_i + \frac{\phi_t}{2}\right)} r_1 \quad (7)$$

and

$$\beta = \alpha \sqrt{1 - \epsilon^2}, \quad (8)$$

where

$$\epsilon = \frac{\sin(\theta_i)}{\cos\left(\frac{\phi_t}{2}\right)}. \quad (9)$$

Moreover, r_1 denotes the distance between the center of the TX and the center of the TX footprint at the RIS plane, while θ_i is the incident angle at the RIS with respect to its broadside direction.

Proof: For brevity, the proof is provided in Appendix A. ■

Based on (7) and (8), the TX beam footprint at the RIS plane can be evaluated as

$$S_i = \pi \alpha \beta. \quad (10)$$

The power that is reflected by the RIS is the one that falls within

$$S = \min(S_i, S_{\text{RIS}}), \quad (11)$$

where S_{RIS} denotes the RIS area. If $S_{\text{RIS}} \leq S_i$, only part of the power that falls within S_{RIS} can be reflected towards the RX; thus, beam waste occurs. On the other hand, if $S_{\text{RIS}} > S_i$ only part of the RIS is used to reflect the incident electromagnetic wave; thus, the RIS gain is decreased.

B. End-to-end SNR

The following proposition returns a tight approximation for the received power.

Proposition 1: The received power can be evaluated as

$$P_r \approx \frac{2.22\Gamma^2 S^2 e_t e_r \gamma^2 \lambda^4}{256 d_x^2 d_y^2 \phi_t^2 \phi_r^2 r_1^2 r_2^2} \cos^p(\theta_i) \cos^p(\theta_r) P_t, \quad (12)$$

where r_2 denotes the distance between the center of the TX footprint at the RIS plane and the center of the RX and Γ stands for the amplitude reflection coefficient of each RU for which it holds

$$\Gamma_n = \Gamma e^{j\theta_n}, \quad (13)$$

where Γ_n stands for the complex reflection coefficient of the n -th illuminated RU and θ_n is the phase it induces.

Proof: For brevity, the proof is provided in Appendix B. ■

Based on (11) and (12), for the case in which $S_{\text{RIS}} < S_i$, (12) can be simplified as

$$P_r^{\text{RIS}} \approx \left(\frac{\lambda^4}{256}\right) \frac{2.22 P_t \Gamma^2 S_{\text{RIS}}^2 e_t e_r \gamma^2}{d_x^2 d_y^2 \phi_t^2 \phi_r^2 r_1^2 r_2^2} \cos^p(\theta_i) \cos^p(\theta_r). \quad (14)$$

Moreover, the beam waste, which is defined as the percentage of energy being lost due to the RIS size being smaller than the illuminated area, can be evaluated as

$$\epsilon_w = 1 - \frac{S_{\text{RIS}}}{S_i}, \quad (15)$$

or, based on (7)–(10),

$$\epsilon_w = 1 - \frac{S_{\text{RIS}}}{\pi \frac{\sin^2\left(\frac{\phi_t}{2}\right) r_1^2}{\cos^2\left(\frac{\phi_t}{2} + \theta_i\right)} \sqrt{1 - \frac{\sin^2(\theta_i)}{\cos^2\left(\frac{\phi_t}{2}\right)}}}. \quad (16)$$

Finally, the end-to-end SNR can be evaluated as

$$\rho_{\text{RIS}} = \frac{P_r}{N_0}, \quad (17)$$

or, equivalently,

$$\rho_{\text{RIS}} \approx \left(\frac{\lambda^4}{256}\right) \frac{2.22 P_t \Gamma^2 S_{\text{RIS}}^2 e_t e_r \gamma^2}{d_x^2 d_y^2 \phi_t^2 \phi_r^2 r_1^2 r_2^2 N_0} \cos^p(\theta_i) \cos^p(\theta_r). \quad (18)$$

On the other hand, for the case in which $S_{\text{RIS}} > S_i$, from (12) and (11), we can evaluate the received power as in (19), given at the top of the following page. Consequently, the equivalent end-to-end SNR at the RX can be approximated as in (20), given at the top of the following page.

IV. OPTIMAL RIS PLACEMENT

This section is focused on identifying the optimal RIS placement in respect to the TX and RX position that maximizes the end-to-end SNR. Let us denote by $r_{1,h}$, $r_{2,h}$, and r_h the horizontal TX-RIS, RIS-RX, and TX-RX distances, respectively, and by h_t , h_{RIS} and h_r the TX, RIS, and RX

$$P_r^i \approx \left(\frac{\lambda^4}{256} \right) \frac{2.22 P_t \Gamma^2 e_t e_r \gamma^2}{d_x^2 d_y^2 \phi_t^2 \phi_r^2} \left(\frac{r_1}{r_2} \right)^2 \cos^p(\theta_i) \cos^p(\theta_r) \pi^2 \frac{\sin^4\left(\frac{\phi_t}{2}\right)}{\cos^4\left(\frac{\phi_t}{2} + \theta_i\right)} \left(1 - \frac{\sin^2(\theta_i)}{\cos^2\left(\frac{\phi_t}{2}\right)} \right) \quad (19)$$

$$\rho_i \approx \left(\frac{\lambda^4}{256} \right) \frac{2.22 P_t \Gamma^2 e_t e_r \gamma^2}{d_x^2 d_y^2 \phi_t^2 \phi_r^2 N_0} \left(\frac{r_1}{r_2} \right)^2 \cos^p(\theta_i) \cos^p(\theta_r) \pi^2 \frac{\sin^4\left(\frac{\phi_t}{2}\right)}{\cos^4\left(\frac{\phi_t}{2} + \theta_i\right)} \left(1 - \frac{\sin^2(\theta_i)}{\cos^2\left(\frac{\phi_t}{2}\right)} \right) \quad (20)$$

heights, respectively. Then, r_1 , r_2 , θ_i , and θ_r can be expressed and as

$$r_1 = \sqrt{r_{1,h}^2 + (h_{\text{RIS}} - h_t)^2}, \quad (21)$$

$$r_2 = \sqrt{(r_h - r_{1,h})^2 + (h_{\text{RIS}} - h_r)^2}, \quad (22)$$

$$\theta_i = \tan^{-1} \left(\frac{|r_{1,h}|}{h_{\text{RIS}} - h_t} \right) \quad (23)$$

and

$$\theta_r = \tan^{-1} \left(\frac{|r_h - r_{1,h}|}{h_{\text{RIS}} - h_r} \right). \quad (24)$$

Next, for the $S_{\text{RIS}} \leq S_i$ and $S_{\text{RIS}} > S_i$ cases, we determine the $r_{1,h}$ that maximizes the end-to-end SNR.

$S_{\text{RIS}} \leq S_i$: In this case, apart from the end-to-end SNR maximization, we additionally aim at minimizing the beam waste. In this direction, the following proposition returns the optimum TX-RIS horizontal distance that jointly maximizes the end-to-end SNR and minimizes the beam waste.

Proposition 2: The optimum TX-RIS horizontal distance, denoted by $r_{1,h}^*$, that jointly maximizes the end-to-end SNR and minimizes the beam waste can be obtained as

$$r_{1,h}^* = \frac{r_h - \sqrt{r_h^2 - 4(h_{\text{RIS}} - h_A)^2}}{2}, \quad (25)$$

where $h_t = h_r = h_A$ ¹.

Proof: For brevity, the proof is provided in Appendix C. ■

Remark 1: From (25), it becomes apparent that the RIS should be placed closer to the TX than the RX.

$S_{\text{RIS}} > S_i$: The following proposition returns the optimal RIS placement policy for the $S_{\text{RIS}} > S_i$ case.

Proposition 3: In the $S_{\text{RIS}} > S_i$ case, the optimal RIS placement can be obtained as the solution of

$$ar_{1,h}^3 + br_{1,h}^2 + cr_{1,h} + d = 0, \quad (26)$$

where again we consider $h_t = h_r = h_A$. Of note, in (26),

$$a = 2 - 2p, \quad (27)$$

$$b = (3p - 6)r_{1,h}, \quad (28)$$

$$c = (2 - 2p)(h_{\text{RIS}} - h_A)^2 + (4 - p)r_{1,h}^2 \quad (29)$$

¹In practical scenarios, it is expected that $h_t = h_r$. However, even if $h_t \neq h_r$ holds $r_{1,h}^*$ is approximately given by (25) by setting h_A as the mean value of h_t and h_r .

$$d = (p + 2)(h_{\text{RIS}} - h_A)^2 r_{1,h}. \quad (30)$$

Proof: For brevity, the proof is provided in Appendix D. ■

Corollary 1: In the $S_{\text{RIS}} > S_i$ case, the optimal RIS placement is closer to the RX than the TX.

Proof: For brevity, the proof is provided in Appendix E. ■

Special case: For the special, however realistic case, of $p = 1$, the following Lemma returns the optimal TX-RIS horizontal distance.

Lemma 2: For $p = 1$, the optimal TX-RIS horizontal distance that maximizes the end-to-end SNR can be obtained as

$$r_{1,h}^* = \frac{r_h + \sqrt{r_h^2 + 4(h_{\text{RIS}} - h_A)^2}}{2}. \quad (31)$$

Proof: For brevity, the proof is provided in Appendix F. ■

V. COMPARISON WITH RELAYING

The aim of this section is the performance comparison, in terms of end-to-end SNR, of an RIS-aided link with the corresponding one of its HD and DF relay counterpart, where the optimal placement that results in SNR maximization applies to both cases. Towards this, we first compute the end-to-end SNR of the relay-type communication and, subsequently, we use it to derive its optimal placement that maximizes it. Finally, we compare the resulting maximized SNR formulas of the RIS- and relay-aided links.

As far as the relay antenna type is concerned, we consider that it is of the same type as the transmit and receive antennas, hence a parabolic reflector. Furthermore, for practical reasons we assume that the relay node structure is equipped with two separate antennas of the same size where one is used for reception and the other for transmission. Finally, we consider that the boresight directions of the transmit with the relay receive antenna and of the relay transmit antenna with the receive antenna are aligned.

A. End-to-end SNR and optimal placement of a relay-aided link

The end-to-end communication is performed in two times slots.

In the first time slot, only the communication between the transmit and relay receive antennas is performed. The end-to-end SNR at the relay RX, which we denote by $\rho_{rel}^{(1)}$, is given by

$$\rho_{rel}^{(1)} = \left(\frac{\lambda}{4\pi} \right)^2 \frac{P_t G_t G_{rel}}{r_{1,rel}^2 N_0}, \quad (32)$$

where

$$G_{rel} \approx \left(\frac{1.22\pi}{\phi_{rel}} \right)^2 e_{rel} \quad (33)$$

is the relay antenna gain, ϕ_{rel} is its HPBW, e_{rel} is its aperture efficiency, and $r_{1,rel}$ is the distance between the centers of the transmit and relay receive antennas. It holds that

$$r_{1,rel} = \sqrt{r_{1,rel,h}^2 + (h_{rel} - h_t)^2}, \quad (34)$$

where $r_{1,rel,h}$ is the horizontal transmitter-relay distance and h_{rel} is the height of the relay with respect to the ground.

In the second time slot, only the communication between the relay transmit and receive antennas is performed. The SNR at the relay RX, which we denote by $\rho_{rel}^{(2)}$, is given by

$$\rho_{rel}^{(2)} = \left(\frac{\lambda}{4\pi} \right)^2 \frac{P_t G_r G_{rel}}{r_{2,rel}^2 N_0}, \quad (35)$$

where $r_{2,rel}$ is the distance between the centers of the relay transmit and receive antennas. It holds that

$$r_{2,rel} = \sqrt{(r_h - r_{1,rel,h})^2 + (h_{rel} - h_r)^2}. \quad (36)$$

Based on the DF protocol, the end-to-end SNR, which we denote by $\rho_{rel}^{(DF)}$, is given by

$$\rho_{rel}^{(DF)} = \min \left\{ \rho_{rel}^{(1)}, \rho_{rel}^{(2)} \right\}. \quad (37)$$

It is trivial to prove that the maximum value of $\rho_{rel}^{(DF)}$ at the point $r_{1,rel,h}^*$, which we denote by $\rho_{rel}^{(DF)}(r_{1,rel,h}^*)$, is achieved when the relay is placed in a position for which $\rho_{rel}^{(1)} = \rho_{rel}^{(2)}$ holds. Hence,

$$\rho_{rel}^{(DF)}(r_{1,rel,h}^*) = \rho_{rel}^{(1)} = \rho_{rel}^{(2)}, \quad (38)$$

or equivalently

$$\frac{G_t}{r_{1,rel}^2} = \frac{G_r}{r_{2,rel}^2}. \quad (39)$$

Remark 2: By assuming that $G_t = G_r$, which is considered a realistic assumption, since the relay usually employs the same antenna for reception and transmission, from (39), we observe that the relay position that maximizes $\rho_{rel}^{(DF)}(r_{1,rel,h})$ is the one that satisfies the condition

$$r_{1,rel} = r_{2,rel}. \quad (40)$$

Moreover, if $h_t = h_r$, from (34) and (36), it becomes apparent that (40) can be simplified as

$$r_{1,rel,h}^* = \frac{r_h}{2}. \quad (41)$$

This indicates that the relay should be placed in the middle of the TX-RX horizontal distance.

B. SNR comparison

For obtaining expressions that allow us to acquire important insights and without loss of generality, for the comparison of the RIS and relay-aided links we assume that $\phi_t = \phi_r = \phi_{rel} = \phi_A$, $h_t = h_r = h_A$, and $h_{RIS} = h_{rel} = h_R$. As far as the comparison of these two link types is concerned, for the RIS case we consider the two examined cases of $S_{RIS} \leq S_i$ and $S_{RIS} > S_i$. In addition, we assume that $r_h^2 \gg 4(h_R - h_A)^2$ and $d_x = d_y = \frac{\lambda}{2}$ since this commonly considered adjacent-element distance value substantially reduces mutual coupling among adjacent elements. Hence, it enables an almost independent impedance adjustment of each RU from the corresponding one of its adjacent ones.

$S_{RIS} \leq S_i$: Based on the assumption $r_h^2 \gg 4(h_R - h_A)^2$, for the optimal value $r_{1,h}^*$ that maximizes $\rho_{RIS}(r_{1,h})$ and by taking into account Proposition 2 it holds that $r_{1,h}^* \approx 0$. Based on these, $\rho_{RIS}(r_{1,h}^*)$ can be further approximated as

$$\begin{aligned} \rho_{RIS}(r_{1,h}^*) &\approx \frac{2.22 P_t \Gamma^2 S_{RIS}^2 \gamma^2 e_A^2}{64 r_h^2 (h_R - h_A)^2 \phi_A^4 N_0} \\ &\times \cos^p \left(\tan^{-1} \left(\frac{r_h}{h_R - h_A} \right) \right). \end{aligned} \quad (42)$$

Regarding the relaying case, by combining (37) with (3) and taking into account $r_{1,rel,h}^* = \frac{r_h}{2}$, it holds that

$$\rho_{rel}^{(DF)}(r_{1,rel,h}^*) \approx \frac{P_t \lambda^2 2.22 \pi^2 e_A^2}{4 \phi_A^4 r_h^2}. \quad (43)$$

According to (42) and (43), for the ratio of $\rho_{RIS}(r_{1,h}^*)$ over $\rho_{rel}^{(DF)}(r_{1,rel,h}^*)$, which we denote by $\zeta_{RIS,rel}$, it holds that

$$\begin{aligned} \zeta_{RIS,rel} &= \frac{\rho_{RIS}(r_{1,h}^*)}{\rho_{rel}^{(DF)}(r_{1,rel,h}^*)} \\ &\approx \frac{\Gamma^2 S_{RIS}^2 \gamma^2 \cos^p \left(\tan^{-1} \left(\frac{r_h}{h_R - h_A} \right) \right)}{16 \lambda^2 \pi^2 (h_R - h_A)^2}. \end{aligned} \quad (44)$$

Remark 3: As we observe from (44), $\zeta_{RIS,rel}$ is a monotonically decreasing function of r_h . Hence, even if for some r_h it holds that $\zeta_{RIS,rel} > 1$ as r_h increases there is a threshold value of r_h after which $\zeta_{RIS,rel} < 1$ would hold.

$S_{RIS} > S_i$: Due to the fact that according to Proposition 3 the optimal RIS placement in the $S_{RIS} > S_i$ case is relatively close to the RX and the fact that $r_h^2 \gg 4(h_R - h_A)^2$ according to our assumptions, for the optimal value $r_{1,h}^*$ that maximizes $\rho_i(r_{1,h})$, it holds that $r_{1,h}^* \approx r_h$. Based on this and the fact that $\phi_t \ll 1$, $\rho_i(r_{1,h}^*)$ in (80) can be further approximated as

$$\begin{aligned} \rho_i(r_{1,h}^*) &\approx \frac{2.22 P_t \Gamma^2 e_A^2 \gamma^2 \pi^2 r_h^2}{256 (h_R - h_A)^2 N_0} \\ &\times \cos^{p-2} \left(\tan^{-1} \left(\frac{r_h}{h_R - h_A} \right) \right). \end{aligned} \quad (45)$$

According to (45) and (43), for the ratio of $\rho_i(r_{1,h}^*)$ over $\rho_{rel}^{(DF)}(r_{1,rel,h}^*)$, which we denote by $\zeta_{i,rel}$, it holds that

$$\zeta_{i,rel} = \frac{\rho_i(r_{1,h}^*)}{\rho_{rel}^{(DF)}(r_{1,rel,h}^*)} \approx \frac{\Gamma^2 \gamma^2 r_h^4 \phi_A^4 \cos^{p-2} \left(\tan^{-1} \left(\frac{r_h}{h_R - h_A} \right) \right)}{64 (h_R - h_A)^2 \lambda^2}. \quad (46)$$

Remark 4: Regarding the 1st derivative of $\zeta_{i,rel}$ with respect to r_h , which we denote by $\frac{d\zeta_{i,rel}}{dr_h}$, it holds that

$$\frac{d\zeta_{i,rel}}{dr_h} = \frac{4(h_R - h_A)^2 r_h^3 - (p-6)r_h^5}{64(h_R - h_A)^4 \lambda^2} \times \Gamma^2 \gamma^2 \phi_A^4 \left(\frac{r_h^2}{(h_R - h_A)^2} + 1 \right)^{-\frac{p}{2}} \quad (47)$$

From (47) we observe that $\zeta_{i,rel}$ is a monotonically increasing function of r_h for $p < 6$, which means that under practical implementations $\zeta_{i,rel}$ increases as r_h increases. Furthermore, by direct inspection of (46) we expect that $\zeta_{i,rel} \gg 1$ even for small values of r_h since the numerator scales with r_h^4 , whereas the denominator with λ^2 . Such a claim is validated in Section VI.

VI. NUMERICAL RESULTS & DISCUSSION

The aim of this section is threefold: i) To illustrate how the beam waste is affected by the positioning and the size of the RIS; ii) To validate Propositions 2 and 3 regarding the optimal placement of an RIS in the $S_{RIS} \leq S_i$ and $S_{RIS} > S_i$ cases, respectively; iii) To validate Remarks 3 and 4 regarding end-to-end SNR ratio of the RIS- and relay-aided links. In this direction, for the involved parameters we consider the values of Table II. For the considered parabolic reflector dimension, the HPBW is approximately equal to 0.98° , which complies with the analysis that is based on the pencil-beam assumption.

TABLE II
PARAMETER VALUES USED IN THE SIMULATION.

Parameter	Value
f	140 GHz
P_t	1 W
W	2 GHz
\mathcal{F}_{dB}	10 dB
h_{RIS}, h_{rel}	15 m
h_t, h_r	3 m
D_t, D_r, D_{rel}	15 cm
e_{Tx}, e_{Rx}, e_{rel}	0.7
Γ	0.9
p	0.5

A. Impact of $r_{1,h}$ on ϵ_w

Regarding the behavior of ϵ_w with respect to $r_{1,h}$, in Fig. 2 we illustrate ϵ_w vs. $r_{1,h}$ for $r_h = 40$ m and different S_{RIS} ². As we observe from Fig. 2, ϵ_w , as expected, increases as the RIS is moving towards the RX, since the impinging beam footprint increases. However, the larger S_{RIS} is the larger the range of $r_{1,h}$ is for which $\epsilon_w = 0$ holds. In fact, we observe that for the $S_{RIS} = 1.5 \text{ m}^2$ case it holds that $r_{1,h} = 0$ for $r_{1,h} \leq r_h$.

²Such short r_h distances are foreseen for the mmWave backhaul networks of next-generation ultra-dense small-cell networks [28].

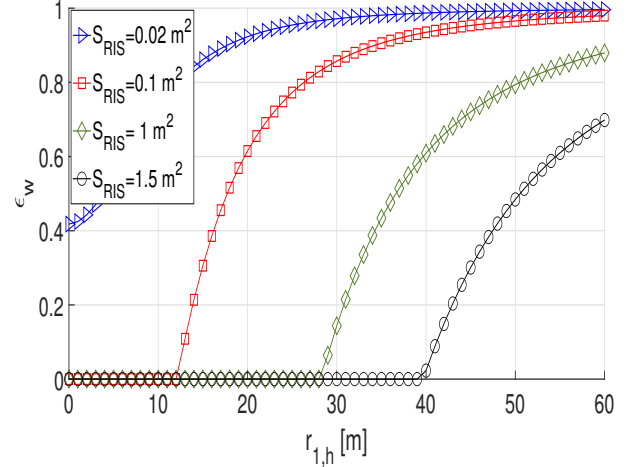


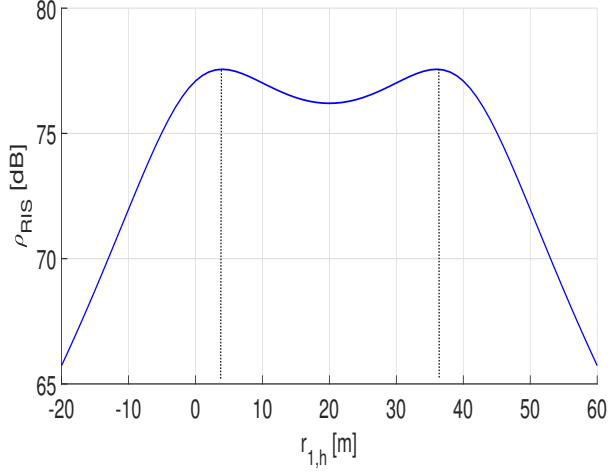
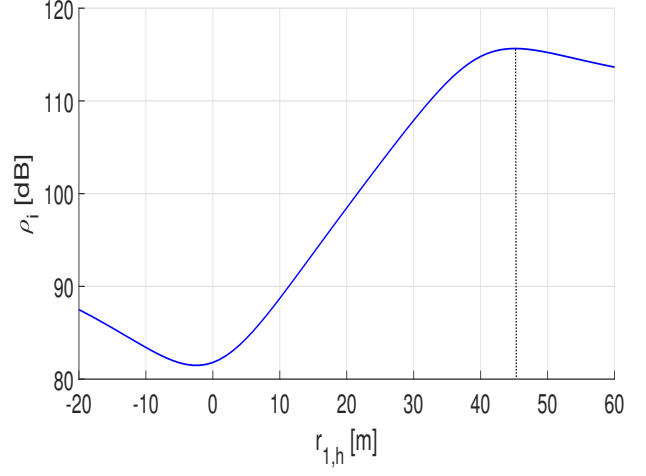
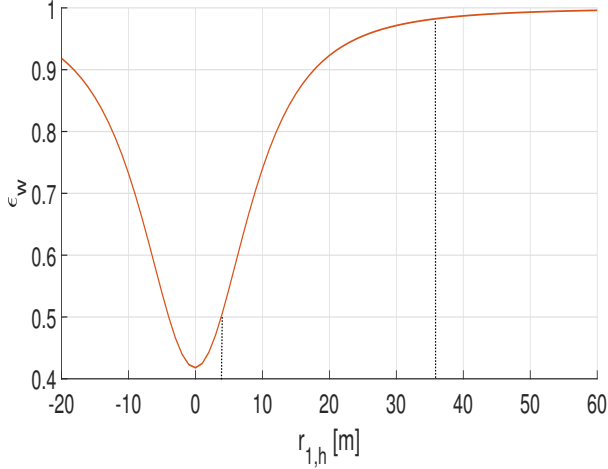
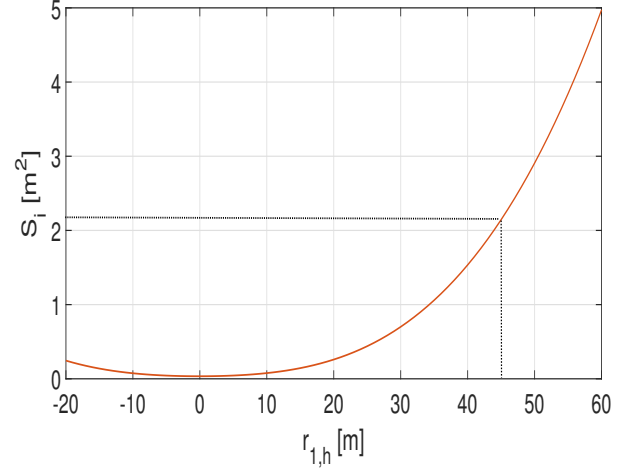
Fig. 2. ϵ_w vs. $r_{1,h}$ for $r_h = 40$ m and different S_{RIS} .

B. Validation of Propositions 2 and 3

As far as the validation of Proposition 2 is concerned, in Fig. 3-(a) and Fig. 3-(b) we depict the ρ_{RIS} vs. $r_{1,h}$ and ϵ_w vs. $r_{1,h}$ curves for $r_h = 40$ m and $S_{RIS} = 0.02 \text{ m}^2$. Such an S_{RIS} value is small enough so that there is a beam waste throughout the examined $r_{1,h}$ range. As we observe from Fig. 3-(a), there are two symmetrical points for which ρ_{RIS} obtains the same maximum value. The 1st point, which is closer to the TX, is at $r_{1,h} = 4$ m and the second point, which is closer to the RX, at $r_{1,h} = 36$ m. However, since ϵ_w is a monotonically increasing function of $r_{1,h}$ for $|r_{1,h}| > 0$, based on (16), and as we observe from Fig. 3-(b), the selected value of $r_{1,h}$ between these two values is $r_{1,h} = 4$ m. Consequently, the RIS should be deployed closer to the TX.

Now, regarding the validation of Proposition 3, in Fig. 4-(a) and Fig. 4-(b) we illustrate the ρ_i vs. $r_{1,h}$ and S_i vs. $r_{1,h}$ curves for $r_h = 40$ by considering that S_{RIS} is sufficiently large so that $S_{RIS} > S_i$. As we observe from Fig. 4-(a), there is only one value of $r_{1,h}$ that maximizes ρ_i , which corresponds to a placement closer to the RX than the TX, as stated in Proposition 3. For the particular point it holds that $r_{1,h} \approx 45$ m and $S_i \approx 2.15 \text{ m}^2$. Hence, to obtain such a behavior of the end-to-end SNR an RIS with an area at least equal to approximately 2.15 m^2 is required. This validates the practicality of such a deployment since such an area can be mounted on the facades of large structures, such as buildings.

In addition, in Fig. 5-(a) we illustrate the $r_{1,h}^*$ vs. S_{RIS} curve for $r_h = 40$ m and a scanning range $r_{1,h} \in [-20 \text{ m}, 60 \text{ m}]$. From Fig. 5-(a), we observe the two regions for which $S_{RIS} < S_i(r_{1,h}^*)$ and $S_{RIS} > S_i(r_{1,h}^*)$ hold throughout the scanning range of $r_{1,h}$. In particular, we observe that the $S_{RIS} < S_i(r_{1,h}^*)$ case holds for $S_{RIS} < 0.04 \text{ m}^2$, whereas the $S_{RIS} > S_i(r_{1,h}^*)$ case holds for $S_{RIS} > 2.15 \text{ m}^2$. In addition, we observe that for the $S_{RIS} < S_i(r_{1,h}^*)$ and $S_{RIS} > S_i(r_{1,h}^*)$ regions the RIS should be placed closer to the TX and closer to the RX, respectively, which further validates Propositions 2 and 3, besides the results of Fig. 4. More specifically, for

(a) ρ_{RIS} vs. $r_{1,h}$.(a) ρ_i vs. $r_{1,h}$.(b) ϵ_w vs. $r_{1,h}$.(b) S_i vs. $r_{1,h}$.Fig. 3. ρ_{RIS} and ϵ_w vs. $r_{1,h}$ for $r_h = 40$ m and $S_{\text{RIS}} = 0.02$ m².Fig. 4. ρ_i and S_i vs. $r_{1,h}$ for $r_h = 40$ m.

the $S_{\text{RIS}} < S_i(r_{1,h}^*)$ and $S_{\text{RIS}} > S_i(r_{1,h}^*)$ regions it holds that $r_{1,h}^* = 4$ m and $r_{1,h}^* \approx 44.9$ m, respectively. Finally, in Fig. 5-(b), we illustrate the $\rho(r_{1,h}^*)$ vs. S_{RIS} curve, where $\rho(r_{1,h}^*) \in \{\rho_{\text{RIS}}(r_{1,h}^*), \rho_i(r_{1,h}^*)\}$. As we observe, as S_{RIS} increases $\rho(r_{1,h}^*)$ increases up to the value that corresponds to $S_{\text{RIS}} \approx 2.15$ m² and it subsequently saturates. This is attributed to the fact that any increase of S_{RIS} beyond the point for which $S_{\text{RIS}} = S_i(r_{1,h}^*) \approx 2.15$ m² does not result in an increase in $\rho(r_{1,h}^*)$ since $r_{1,h}^*$ does not change.

C. Validation of Remarks 3 and 4

As far as the validation of Remarks 3 and 4 is concerned, in Fig. 6-(a) we depict the $\zeta_{\text{RIS},\text{rel}}$ vs. r_h curve for $S_{\text{RIS}} = 0.05$ m². We note that for the particular value of S_{RIS} it holds that $S_{\text{RIS}} < S_i(r_{1,h}^*)$ for the examined range of r_h . As we observe, $\zeta_{\text{RIS},\text{rel}}$ monotonically decreases as r_h increases, which validates the analysis based, according to Section V-B, Remark 3. Furthermore, in Fig 6-(b) we depict the $\zeta_{i,\text{rel}}$ vs.

r_h curve for $S_{\text{RIS}} = 10$ m². For the particular value of S_{RIS} it holds that $S_{\text{RIS}} > S_i(r_{1,h}^*)$ for the examined range of r_h . As we observe, $\zeta_{i,\text{rel}}$ monotonically increases as r_h increases, which validates the also analysis based, according to Section V-B, Remark 4. Based on the results depicted in Fig. 6, we conclude that when $S_{\text{RIS}} < S_i(r_{1,h}^*)$ a relay would most likely provide a better performance unless the TX-RX distance is relatively small. On the other hand, for $S_{\text{RIS}} > S_i(r_{1,h}^*)$ a substantial performance gain with respect to a relay is expected. According to the results, the larger the TX-RX distance is, the higher the performance gain is. With respect to this outcome, we again note that the facades of large structures, such as buildings, are the most suitable mounting structures for the required RIS sizes.

VII. CONCLUSIONS

This work has been motivated by the need to answer the question of where an RIS that aids a highly directional mmWave TX-RX link under blockage should be placed. Based on this, we have considered the two cases of the transmit beam

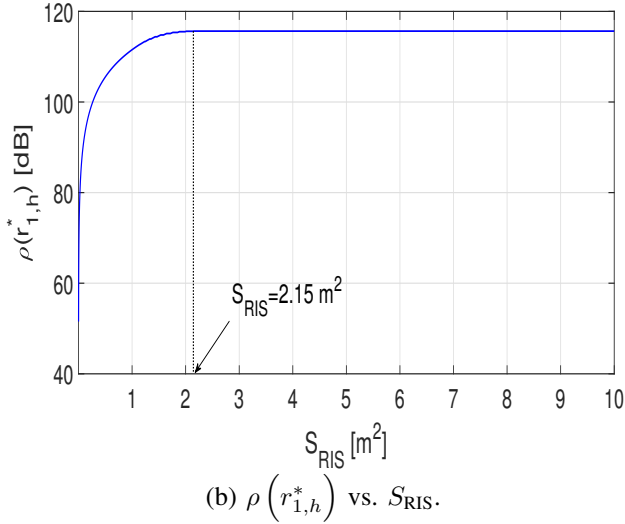
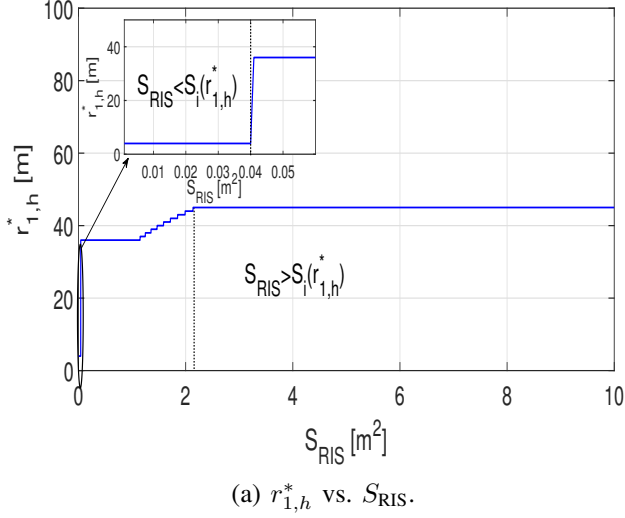


Fig. 5. $r_{1,h}^*$ and $\rho(r_{1,h}^*)$ vs. S_{RIS} for $r_h = 40$ m.

illuminating the entire RIS area in the case of an RIS smaller than the transmit beam footprint on the RIS plane, or only a portion of the RIS area in the case of large RIS structures with areas larger than the particular footprint. For these two cases, we have computed the end-to-end SNR, which enabled us to extract the optimal placement in each of them that maximizes it. In particular, in the case of an RIS smaller than the transmit beam footprint the RIS should be placed closer to the TX so as to minimize the beam waste. On the other hand, in the case of an RIS larger than the footprint a placement closer to the RX is the optimal solution. Equivalently, this network planning optimization can be viewed in a different perspective by considering a future urban scenario in which there is an abundance of buildings coated by RISs. In such a case, depending on the size of the RISs with respect to the transmit beam footprints, the transmitters will be focusing their beams to RISs closer to them or closer to the respective receivers so as to maximize the end-to-end SNR.

Furthermore, we have compared the resulting SNR expressions with the corresponding one of a HD/DF relay aiding the

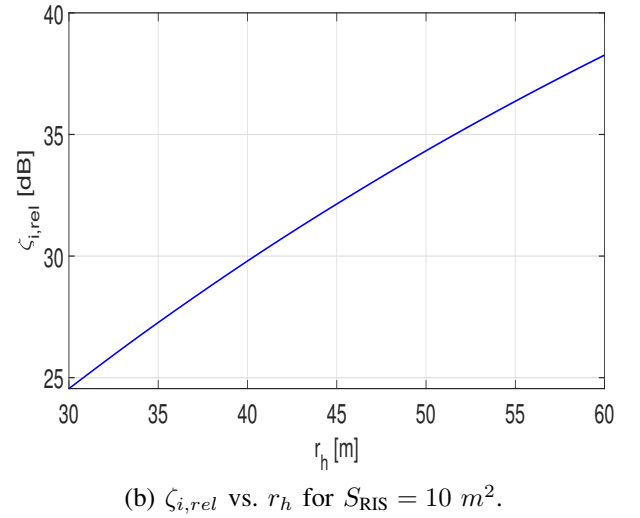
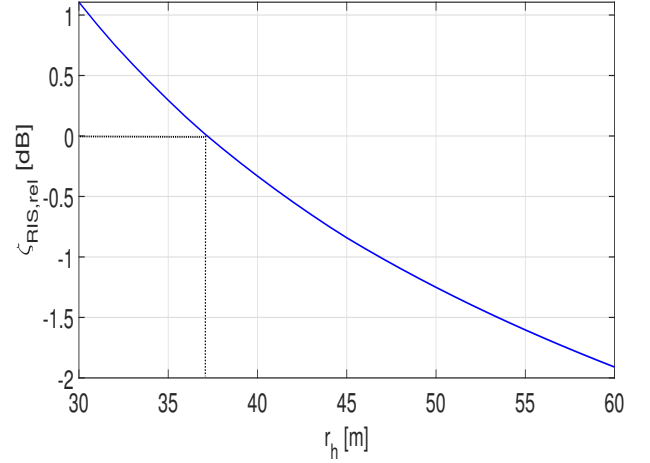


Fig. 6. $\zeta_{RIS,rel}$ and $\zeta_{i,rel}$ vs. r_h .

communication. In particular, for the $S_{RIS} < S_i$ case it was proved that the SNR ratio of the RIS- over the relay-aided link is a monotonically decreasing function of the TX-RX distance. This reveals that there is a threshold value of the particular distance above which the relay-aided link results in a better SNR performance. On the other hand, the corresponding SNR ratio is a monotonically increasing function of the TX-RX distance for the $S_{RIS} > S_i$ case. In addition, the results show that in the particular case even for a small TX-RX distance substantial SNR gains are expected by the RIS deployment compared to the relay-based one.

Finally, we note that although this work has considered links of fixed topology, the presented outcomes are also applicable to mobile networks. For instance, for a mobile user that should be served through an RIS the TX should focus its beam to an RIS mounted on a building close to it in the case of $S_{RIS} < S_i$. On the other hand, the TX should focus its beam to an RIS mounted on a building close to the mobile user in the $S_{RIS} > S_i$ case.

APPENDICES

APPENDIX A

PROOF OF LEMMA 1

By applying the law of sines in the $\triangle ABC$, we obtain

$$\frac{\sin\left(\frac{\phi_t}{2}\right)}{a} = \frac{\sin\left(\widehat{BCA}\right)}{r_1} \quad (48)$$

where \widehat{BCA} can be calculated as

$$\widehat{BCA} = \frac{\pi}{2} - \frac{\phi_t}{2} - \theta_i. \quad (49)$$

By substituting (49) into (48), we obtain (7).

The eccentricity of the elliptical footprint can be evaluated as

$$\epsilon = \frac{\sin(\theta_i)}{\sin\left(\frac{\pi}{2} - \frac{\phi_t}{2}\right)}, \quad (50)$$

or equivalently as in (9). Finally, β can be obtained as in (8). This concludes the proof.

APPENDIX B

PROOF OF PROPOSITION 1

The incident electric field on the n -th RU of the RIS illuminated area can be obtained as

$$\mathbf{E}_{i,n} = E_{i,n} e^{-j\frac{2\pi}{\lambda} r_{t,n}} \mathbf{n}_o, \quad (51)$$

where $r_{t,n}$ is the distance between the TX and the n -th RU of the illuminated RIS area, while $E_{i,n}$ is the amplitude of the incident wave, and \mathbf{n}_o is a unitary vector that is perpendicular to the 2D plane that the electric field lies on [29][Example 11-3]. Of note, since the RIS is placed in the far-field, $E_{i,n} = E_i$ for each $i = 1, \dots, M$, where M represents the number of illuminated RUs in the RIS. It holds

$$M = \frac{S}{d_x d_y}. \quad (52)$$

Moreover, $r_{t,n} \approx r_1$. As a consequence, the power density at the n -th RU of the RIS can be expressed as

$$P_i = \frac{E_i^2}{2\eta} \quad (53)$$

or, with the aid of (51), as

$$P_i = \frac{P_t G_t}{4\pi r_1^2}, \quad (54)$$

where η is the free-space impedance. Thus, the incident power at the n -th RU can be evaluated as

$$P_{i,n} = P_i A, \quad (55)$$

where A stands for the effective aperture of the n -th illuminated RU and can be obtained as

$$A = \frac{\lambda^2}{4\pi} G_{\text{RIS}}(\theta_i). \quad (56)$$

By substituting (54) and (56) into (55), we obtain

$$P_{i,n} = \left(\frac{\lambda}{4\pi}\right)^2 \frac{P_t G_t G_{\text{RIS}}(\theta_i)}{r_1^2}. \quad (57)$$

As a result, and due to the energy conservation law, the reflected power density by the n -th RU, which is captured by the RX antenna, can be expressed as

$$P_{r,n} = \frac{P_{i,n} |\Gamma_n|^2 G_{\text{RIS}}(\theta_r)}{4\pi r_2^2}, \quad (58)$$

By substituting (57) and (13) into (58), we obtain

$$P_{r,n} = \frac{\lambda^2}{(4\pi)^3} \frac{P_t \Gamma^2 G_t G_{\text{RIS}}(\theta_i) G_{\text{RIS}}(\theta_r)}{r_1^2 r_2^2}. \quad (59)$$

Moreover, the corresponding electric field can be evaluated as

$$\mathbf{E}_{r,n} = E_{r,n} e^{-j\left(\theta_n + \frac{2\pi(r_{t,n} + r_{n,r})}{\lambda}\right)} \mathbf{a}_o, \quad (60)$$

where $r_{n,r}$ is the distance between the n -th illuminated RU and the RX and \mathbf{a}_o is a unitary vector perpendicular to the 2D plane that the reflected electric field lies on. Additionally, $E_{r,n}$ can be computed as

$$E_{r,n} = \sqrt{2\eta P_{r,n}}, \quad (61)$$

which, by employing (59), can be rewritten as

$$E_{r,n} = \sqrt{\frac{2\eta \lambda^2}{(4\pi)^3} \frac{P_t \Gamma^2 G_t G_{\text{RIS}}(\theta_i) G_{\text{RIS}}(\theta_r)}{r_1^2 r_2^2}}. \quad (62)$$

From (60), the aggregated electric field at the RX can be written as

$$\mathbf{E}_r = \sum_{n=1}^M \mathbf{E}_{r,n}. \quad (63)$$

Consequently, by employing (60) and (62) it holds that

$$\mathbf{E}_r = \sqrt{\frac{2\eta \lambda^2}{(4\pi)^3} \frac{P_t \Gamma^2 G_t G_{\text{RIS}}(\theta_i) G_{\text{RIS}}(\theta_r)}{r_1^2 r_2^2}} \delta \mathbf{a}_o, \quad (64)$$

where

$$\delta = \sum_{n=1}^M e^{-j\left(\theta_n + \frac{2\pi(r_{t,n} + r_{n,r})}{\lambda}\right)}. \quad (65)$$

Hence, at the RX, the received power can be obtained as

$$P_r = \frac{|\mathbf{E}_r|^2}{2\eta} \frac{\lambda^2}{4\pi} G_r, \quad (66)$$

which, with the aid of (64), can be rewritten as

$$P_r = \left(\frac{\lambda}{4\pi}\right)^4 \frac{\Gamma^2 G_t G_r G_{\text{RIS}}(\theta_i) G_{\text{RIS}}(\theta_r)}{r_1^2 r_2^2} |\delta|^2 P_t. \quad (67)$$

By assuming that the optimal phase shift is induced by each RU so as to maximize P_r , i.e.,

$$\theta_n = -\frac{2\pi(r_{t,n} + r_{n,r})}{\lambda}, \quad (68)$$

the received power can be rewritten as

$$P_r = \left(\frac{\lambda}{4\pi}\right)^4 \frac{\Gamma^2 G_t G_r G_{\text{RIS}}(\theta_i) G_{\text{RIS}}(\theta_r)}{r_1^2 r_2^2} M^2, \quad (69)$$

which can be equivalently written as in (12). This concludes the proof.

APPENDIX C

PROOF OF PROPOSITION 2

The proof begins by rewriting (18) as

$$\rho_{\text{RIS}} \approx \left(\frac{\lambda^4}{256} \right) \frac{2.22 P_t \Gamma^2 S_{\text{RIS}}^2 e_t e_r \gamma^2 F(r_{1,h})}{d_x^2 d_y^2 \phi_t^2 \phi_r^2 N_0 G(r_{1,h})}, \quad (70)$$

where

$$F(r_{1,h}) = \cos^p \left(\tan^{-1} \left(\frac{|r_{1,h}|}{h_{\text{RIS}} - h_A} \right) \right) \times \cos^p \left(\tan^{-1} \left(\frac{|r_h - r_{1,h}|}{h_{\text{RIS}} - h_A} \right) \right) \quad (71)$$

and

$$G(r_{1,h}) = \left(r_{1,h}^2 + (h_{\text{RIS}} - h_A)^2 \right) \times \left((r_h - r_{1,h})^2 + (h_{\text{RIS}} - h_A)^2 \right). \quad (72)$$

From (70), we observe that the end-to-end SNR depends on $r_{1,h}$ through the ratio $\frac{F(r_{1,h})}{G(r_{1,h})}$. Hence, the optimum $r_{1,h}$ that maximizes ρ_{RIS} can be obtained by evaluating the roots of the first derivative of $\frac{F(r_{1,h})}{G(r_{1,h})}$ with respect to $r_{1,h}$. The first derivative of $\frac{F(r_{1,h})}{G(r_{1,h})}$ can be obtained as in (73), given at the top of the following page. In (73),

$$C = ((h_{\text{RIS}} - h_A)^2 + r_{1,h}^2)^2 ((h_{\text{RIS}} - h_A)^2 + (r_h - r_{1,h})^2)^2. \quad (74)$$

The three real roots of (73) can be obtained as

$$r_{1,h}^{(1)} = \frac{r_h}{2} \quad (75)$$

$$r_{1,h}^{(2)} = \frac{r_h - \sqrt{r_h^2 - 4(h_{\text{RIS}} - h_A)^2}}{2}. \quad (76)$$

and

$$r_{1,h}^{(3)} = \frac{r_h + \sqrt{r_h^2 - 4(h_{\text{RIS}} - h_A)^2}}{2}. \quad (77)$$

Notice that $r_{1,h}^{(1)}$ minimizes (70), whereas $r_{1,h}^{(2)}$ and $r_{1,h}^{(3)}$ maximize it with the same maximum value obtained.

As far as the minimization of $\epsilon_w(r_{1,h})$ is concerned, from (9) it holds that

$$\epsilon_w(r_{1,h}) \approx 1 - \frac{S_{\text{RIS}}}{\pi \frac{\sin^2(\frac{\phi_t}{2})(r_{1,h}^2 + (h_{\text{RIS}} - h_A)^2)}{\cos \left(\tan^{-1} \left(\frac{|r_{1,h}|}{h_{\text{RIS}} - h_A} \right) \right)}}, \quad (78)$$

where, in (78), we assumed that $\frac{\phi_t}{2}$ is relative small, due to pencil-beam transmission, and we use the approximations $\cos \left(\frac{\phi_t}{2} \right) \approx 1$ and $\tan^{-1} \left(\frac{|r_{1,h}|}{h_{\text{RIS}} - h_t} \right) \gg \frac{\phi_t}{2}$. From (78), it is trivial to prove that $\epsilon_w(r_{1,h})$ is a monotonically increasing function of $r_{1,h}$. Hence, for the roots $r_{1,h}^{(2)}$ and $r_{1,h}^{(3)}$, since $r_{1,h}^{(2)} < r_{1,h}^{(3)}$, it holds that $\epsilon_w(r_{1,h}^{(2)}) < \epsilon_w(r_{1,h}^{(3)})$. Physically, this is justified by the fact that as the RIS moves away from the TX S_i increases; thus, for a fixed S_{RIS} , the beam waste also increases. Consequently,

$$r_{1,h}^* = r_{1,h}^{(2)}. \quad (79)$$

This concludes the proof.

APPENDIX D

PROOF OF PROPOSITION 3

As a function of $r_{1,h}$, the end-to-end SNR can be approximated as

$$\rho_i(r_{1,h}) \approx \left(\frac{\lambda^4}{256} \right) \frac{2.22 P_t \Gamma^2 e_t e_r \gamma^2}{d_x^2 d_y^2 \phi_t^2 \phi_r^2 N_0} \pi^2 \sin^4 \left(\frac{\phi_t}{2} \right) H(r_{1,h}), \quad (80)$$

where $H(r_{1,h})$ can be obtained as in (81), given at the top of the next page.

According to (80), $\rho_i(r_{1,h})$ depends on $r_{1,h}$ through $H(r_{1,h})$. Hence, the values of $r_{1,h}$ that maximize $\rho_i(r_{1,h})$ are obtained by finding the roots of the first derivative of $H(r_{1,h})$ with respect to $r_{1,h}$. In this direction, after taking into account that $\cos \left(\frac{\phi_t}{2} \right) \approx 1$ and $\tan^{-1} \left(\frac{|r_{1,h}|}{h_{\text{RIS}} - h_A} \right) \gg \frac{\phi_t}{2}$, by considering that $\frac{\phi_t}{2} \ll 1$, due to pencil-beam transmission, we can approximate (81) as in (82), given at the top of the following page. The derivative of $H(r_{1,h})$ can be obtained as

$$\frac{dH(r_{1,h})}{dr_{1,h}} = \frac{ar_{1,h}^3 + br_{1,h}^2 + cr_{1,h} + d}{K} \quad (83)$$

where a , b , c , and d are given by (27)–(30), while

$$K = \left((h_{\text{RIS}} - h_A)^2 + r_{1,h}^2 \right) \left(\frac{r_{1,h}^2}{(h_{\text{RIS}} - h_A)^2} + 1 \right)^{\frac{p}{2}} \times (h_{\text{RIS}} - h_A)^2 \left(\frac{(r_{1,h} - r_{1,h})^2}{(h_{\text{RIS}} - h_A)^2} + 1 \right)^{\frac{p}{2}} \times \left((h_{\text{RIS}} - h_A)^2 + r_{1,h}^2 - 2r_h r_{1,h} + r_{1,h}^2 \right)^2. \quad (84)$$

Consequently, the roots of $\frac{dH(r_{1,h})}{dr_{1,h}}$ are the roots of the cubic polynomial

$$J(r_{1,h}) = ar_{1,h}^3 + br_{1,h}^2 + cr_{1,h} + d. \quad (85)$$

This concludes the proof.

APPENDIX E

PROOF OF COROLLARY 1

The discriminant of the polynomial that is given in (85) can be evaluated as

$$\Delta = \frac{t_1^3}{27} + \frac{t_2^2}{4}, \quad (86)$$

where

$$t_1 = \frac{c}{a} - \frac{b^2}{3a^2} \quad (87)$$

and

$$t_2 = \frac{2b^3}{27a^3} - \frac{bc}{3a^2} + d. \quad (88)$$

$$\frac{d\left(\frac{F(r_{1,h})}{G(r_{1,h})}\right)}{dr_{1,h}} = \frac{(r_h - 2r_{1,h})}{C} \left(r_{1,h}^2 - r_h r_{1,h} + (h_{\text{RIS}} - h_A)^2 \right) (p+2) \left(\frac{r_{1,h}^2}{(h_{\text{RIS}} - h_A)^2} + 1 \right)^{-\frac{p}{2}} \left(\frac{(r_h - r_{1,h})^2}{(h_{\text{RIS}} - h_A)^2} + 1 \right)^{-\frac{p}{2}} \quad (73)$$

$$H(r_{1,h}) = \frac{r_{1,h}^2 + (h_{\text{RIS}} - h_t)^2}{(r_h - r_{1,h})^2 + (h_{\text{RIS}} - h_r)^2} F(r_{1,h}) \frac{1 - \frac{\sin^2\left(\tan^{-1}\left(\frac{|r_{1,h}|}{h_{\text{RIS}} - h_t}\right)\right)}{\cos^2\left(\frac{\phi_t}{2}\right)}}{\cos^4\left(\frac{\phi_t}{2} + \tan^{-1}\left(\frac{|r_{1,h}|}{h_{\text{RIS}} - h_t}\right)\right)}. \quad (81)$$

$$H(r_{1,h}) \approx \frac{r_{1,h}^2 + (h_{\text{RIS}} - h_t)^2}{(r_{1,h} - r_{1,h})^2 + (h_{\text{RIS}} - h_r)^2} \cos^{p-2}\left(\tan^{-1}\left(\frac{|r_{1,h}|}{h_{\text{RIS}} - h_t}\right)\right) \cos^p\left(\tan^{-1}\left(\frac{|r_h - r_{1,h}|}{h_{\text{RIS}} - h_r}\right)\right) \quad (82)$$

If $\Delta < 0$, the cubic polynomial returns the following three real roots:

$$\tilde{r}_{1,h}^{(1)} = \frac{2}{\sqrt{3}} \sqrt{-t_1} \sin\left(\frac{1}{3} \sin^{-1}\left(\frac{3\sqrt{3}t_2}{2(\sqrt{-t_1})^3}\right)\right) - \frac{b}{3a}, \quad (89)$$

$$\tilde{r}_{1,h}^{(2)} = -\frac{2}{\sqrt{3}} \sqrt{-t_1} \sin\left(\frac{1}{3} \sin^{-1}\left(\frac{3\sqrt{3}t_2}{2(\sqrt{-t_1})^3}\right) + \frac{\pi}{3}\right) - \frac{b}{3a}, \quad (90)$$

and

$$\tilde{r}_{1,h}^{(3)} = \frac{2}{\sqrt{3}} \sqrt{-t_1} \cos\left(\frac{1}{3} \sin^{-1}\left(\frac{3\sqrt{3}t_2}{2(\sqrt{-t_1})^3}\right) + \frac{\pi}{6}\right) - \frac{b}{3a}. \quad (91)$$

If $\Delta > 0$, there is only one real root that can be obtained as

$$\tilde{r}_{1,h}^{(4)} = \left(-\frac{t_2}{2} + \sqrt{\Delta}\right)^{\frac{1}{3}} + \left(-\frac{t_2}{2} - \sqrt{\Delta}\right)^{\frac{1}{3}} - \frac{b}{3a}. \quad (92)$$

Finally, if $\Delta = 0$, the 3 real roots are

$$\tilde{r}_{1,h}^{(5)} = -2\left(\frac{t_2}{2}\right)^{\frac{1}{3}} - \frac{b}{3a} \quad (93)$$

$$\tilde{r}_{1,h}^{(6,7)} = \left(\frac{t_2}{2}\right)^{\frac{1}{3}} - \frac{b}{3a}. \quad (94)$$

In all 3 different cases of Δ one of the roots maximizes $H(r_{1,h})$, while the others minimize it. This solution imposes the RIS to be closer to the RX than the TX, in order to exploit the maximum number of RIS's RUs. In Fig. 7, we illustrate the value of $r_{1,h}$, denoted by $r_{1,h}^*$, that maximizes $H(r_{1,h})$ as a function of p . As we observe from Fig. 7, throughout the range of p the optimal value of $r_{1,h}$ is relatively close to r_h , which means that the RIS should optimally be placed closer to the RX than the TX. This concludes the proof.

APPENDIX F

PROOF OF LEMMA 2

For the special case in which $p = 1$, (83) reduces to a second order polynomial with roots that are given by (31).

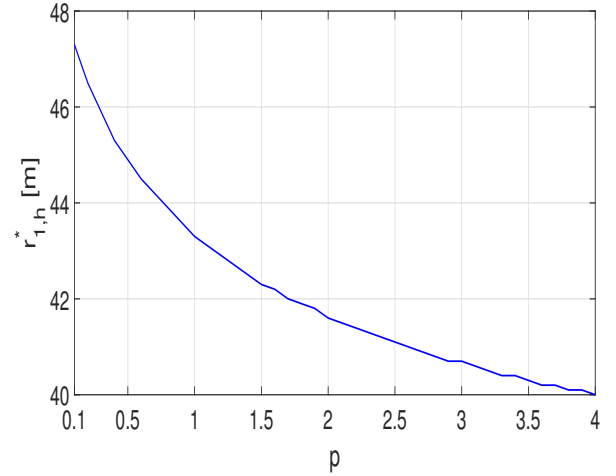


Fig. 7. $r_{1,h}^*$ vs. p for $r_h = 40$ m, $h_{\text{RIS}} = 15$ m, and $h_A = 3$ m.

For these roots, it can be seen through the second-derivative test that the negative root (RIS located closer to the TX than the RX) minimizes $H(r_{1,h})$, whereas the positive root (RIS located closer to the RX than the TX) maximizes it.

REFERENCES

- [1] "Mobile backhaul options: Spectrum analysis and recommendations," ABI Research, Tech. Rep., Sep. 2018.
- [2] "Millimetre wave transmission (mwt); analysis of spectrum, license schemes and network scenarios in the d-band," ETSI, Tech. Rep., Aug. 2018.
- [3] M. R. Akdeniz, Y. Liu, M. K. Samimi, S. Sun, S. Rangan, T. S. Rappaport, and E. Erkip, "Millimeter Wave Channel Modeling and Cellular Capacity Evaluation," *IEEE J. Sel. Areas Commun.*, vol. 32, no. 6, pp. 1164–1179, June 2014.
- [4] T. S. Rappaport, S. Sun, R. Mayzus, H. Zhao, Y. Azar, K. Wang, G. N. Wong, J. K. Schulz, M. Samimi, and F. Gutierrez, "Millimeter Wave Mobile Communications for 5G Cellular: It Will Work!" *IEEE Access*, vol. 1, pp. 335–349, May 2013.
- [5] J. N. Laneman, D. N. C. Tse, and G. W. Wornell, "Cooperative diversity in wireless networks: Efficient protocols and outage behavior," *IEEE Trans. Inf. Theory*, vol. 50, no. 12, pp. 3062–3080, Dec. 2004.
- [6] W. Khawaja, O. Ozdemir, Y. Yapici, F. Erden, and I. Guvenc, "Coverage Enhancement for NLOS mmwave Links Using Passive Reflectors," *IEEE Open Journal of the Communications Society*, vol. 1, pp. 263–281, 2020.

- [7] M. T. Barros, R. Mullins, and S. Balasubramaniam, "Integrated Terahertz Communication With Reflectors for 5g Small-Cell Networks," *IEEE Trans. Veh. Tech.*, vol. 66, no. 7, pp. 5647–5657, July 2017.
- [8] Q. Wu and R. Zhang, "Beamforming optimization for intelligent reflecting surface with discrete phase shifts," in *IEEE International Conference on Acoustics, Speech and Signal Processing (ICASSP)*, 2019, pp. 7830–7833.
- [9] —, "Towards smart and reconfigurable environment: Intelligent reflecting surface aided wireless network," *IEEE Commun. Mag.*, vol. 58, no. 1, Nov. 2020.
- [10] O. Özdoğan, E. Björnson, and E. G. Larsson, "Intelligent reflecting surfaces: Physics, propagation, and pathloss modeling," *IEEE Wirel. Commun. Lett.*, vol. 9, no. 5, pp. 581–585, 2020.
- [11] A. A. Boulogeorgos and A. Alexiou, "Performance Analysis of Reconfigurable Intelligent Surface-Assisted Wireless Systems and Comparison With Relaying," *IEEE Access*, vol. 8, May 2020.
- [12] S. Kisseleff, W. A. Martins, H. Al-Hraishawi, S. Chatzinotas, and B. Ottersten, "Reconfigurable Surfaces for Smart Cities: Research Challenges and Opportunities," *IEEE Open Journal of the Communications Society*, to appear.
- [13] E. Basar, M. D. Renzo, J. de Rosny, M.-S. Alouini, and R. Zhang, "Wireless Communications Through Reconfigurable Intelligent Surfaces," *IEEE Access*, vol. 7, pp. 116 753–116 773, Aug. 2019.
- [14] L. Bariah, L. Mohjazi, S. Muhaidat, P. C. Sofotasios, G. K. Kurt, H. Yanikomeroglu, and O. A. Dobre, "A prospective look: Key enabling technologies, applications and open research topics in 6g networks," *ArXiv*, Sep. 2020.
- [15] Q. Wu and R. Zhang, "Intelligent reflecting surface enhanced wireless network via joint active and passive beamforming," *IEEE Trans. Wireless Commun.*, vol. 18, no. 11, pp. 5394–5409, Nov. 2019.
- [16] M. Jung, W. Saad, Y. Jang, G. Kong, and S. Choi, "Performance analysis of large intelligent surfaces (LISs): Asymptotic data rate and channel hardening effects," *IEEE Trans. Wireless Commun.*, vol. 19, no. 3, pp. 2052–2065, Mar. 2020.
- [17] S. Zeng, H. Zhang, B. Di, Z. Han, and L. Song, "Reconfigurable intelligent surface (RIS) assisted wireless coverage extension: RIS orientation and location optimization," *IEEE Commun. Lett.*, pp. 1–1, Nov. 2020.
- [18] M. D. Renzo, K. Ntontin, J. Song, F. H. Danufane, X. Qian, F. Lazarakis, J. D. Rosny, D.-T. Phan-Huy, O. Simeone, R. Zhang, M. Debbah, G. Lerosy, M. Fink, S. Tretakov, and S. Shamai, "Reconfigurable intelligent surfaces vs. relaying: Differences, similarities, and performance comparison," *IEEE Open Journal of the Communications Society*, vol. 1, pp. 798–807, Jun. 2020.
- [19] C. Huang, A. Zappone, G. C. Alexandropoulos, M. Debbah, and C. Yuen, "Wireless Communications Through Reconfigurable Intelligent Surfaces," *IEEE Trans. Wirel. Commun.*, vol. 18, no. 8, pp. 4157–4170, Aug. 2019.
- [20] E. Björnson, O. Özdoğan, and E. G. Larsson, "Intelligent Reflecting Surface vs. Decode-and-Forward: How Large Surfaces Are Needed to Beat Relaying?" *IEEE Wirel. Commun. Lett.*, to appear.
- [21] H. Anderson, *Fixed broadband wireless system design*. Chichester, West Sussex, England Hoboken, NJ: John Wiley & Sons, 2003.
- [22] D. Schulz, V. Jungnickel, C. Alexakis, M. Schlosser, J. Hilt, A. Paraskevopoulos, L. Grobe, P. Farkas, and R. Freund, "Robust optical wireless link for the backhaul and fronthaul of small radio cells," *Journal of Lightwave Technology*, vol. 34, no. 6, pp. 1523–1532, 2016.
- [23] S. Silver, *Microwave antenna theory and design*. London, UK: P. Peregrinus on behalf of the Institution of Electrical Engineers, 1984.
- [24] J. Kraus, *Antennas for all applications*. New York: McGraw-Hill, 2002.
- [25] S. W. Ellingson, "Path Loss in Reconfigurable Intelligent Surface-Enabled Channels," *arXiv:1912.06759*.
- [26] K. Ntontin, M. Di Renzo, and C. Verikoukis, "On the Feasibility of Full-Duplex Relaying in Multiple-Antenna Cellular Networks," *IEEE Trans. Commun.*, vol. 65, no. 5, pp. 2234–2249, May 2017.
- [27] D. Hilbert and S. Cohn-Vossen, *Geometry and the imagination*. New York: Chelsea Publishing Company, 1952.
- [28] S. Saadat, D. Chen, and T. Jiang, "Multipath multihop mmWave backhaul in ultra-dense small-cell network," *Digital Communications and Networks*, vol. 4, no. 2, pp. 111–117, Apr. 2018.
- [29] C. Balanis, *Advanced engineering electromagnetics*. Hoboken, N.J: John Wiley & Sons, 2012.



Konstantinos Ntontin (S'12-M'14) is currently a research associate of the SIGCOM Research Group at SnT, University of Luxembourg, and a research collaborator with the Institute of Informatics and Telecommunications of the National Centre for Scientific research—"Demokritos". In the past, he held research associate positions at the Electronic Engineering and Telecommunications department of the University of Barcelona and at the Informatics and Telecommunications department of the University of Athens. In addition, he held an internship position at Ericsson Eurolab GmbH, Germany. He received the Diploma in Electrical and Computer Engineering in 2006, the M. Sc. Degree in Wireless Systems in 2009, and the Ph. D. degree in 2015 from the University of Patras, Greece, the Royal Institute of Technology (KTH), Sweden, and the Technical University of Catalonia (UPC), Spain, respectively. His research interests are related to the physical layer of wireless telecommunications with focus on performance analysis in fading channels, MIMO systems, array beamforming, transceiver design, and stochastic modeling of wireless channels.



Alexandros-Apostolos A. Boulogeorgos (S'11, M'16, SM'19) was born in Trikala, Greece in 1988. He received the Electrical and Computer Engineering (ECE) diploma degree and Ph.D. degree in Wireless Communications from the Aristotle University of Thessaloniki (AUTH) in 2012 and 2016, respectively.

From November 2012, he has been a member of the wireless communications system group of AUTH, working as a research assistant/project engineer in various telecommunication and networks projects.

During 2017, he joined the information technologies institute, while from November 2017, he has joined the Department of Digital Systems, University of Piraeus, where he conducts research in the area of wireless communications. Moreover, from October 2012 until September 2016, he was a teaching assistant at the department of ECE of AUTH, whereas, from February 2017, he serves as an adjunct lecturer at the Department of Informatics and Telecommunications Engineering of the University of Western Macedonia and as an visiting lecturer at the Department of Computer Science and Biomedical Informatics of the University of Thessaly.

Dr. Boulogeorgos has authored and co-authored more than 50 technical papers, which were published in scientific journals and presented at prestigious international conferences. Furthermore, he has submitted two (one national and one European) patents. Likewise, he has been involved as member of Technical Program Committees in several IEEE and non-IEEE conferences and served as a reviewer in various IEEE journals and conferences. Dr. Boulogeorgos was awarded with the "Distinction Scholarship Award" of the Research Committee of AUTH for the year 2014 and was recognized as an exemplary reviewer for IEEE Communication Letters for 2016 (top 3% of reviewers). Moreover, he was named a top peer reviewer (top 1% of reviewers) in Cross-Field and Computer Science in the Global Peer Review Awards 2019, which was presented by the Web of Science and Publons. His current research interests spans in the area of wireless communications and networks with emphasis in high frequency communications, optical wireless communications and communications for biomedical applications. He is a Senior Member of the IEEE and a member of the Technical Chamber of Greece. He is currently an Editor for IEEE Communications Letters, and an Associate Editor for the Frontier In Communications And Networks.



Dimitrios G. Selimis (S'20) received his Diploma degree in Electrical and Computer Engineering from the University of Patras, Greece, in 2018. He received his master degree in Modern Wireless Communications from University of Peloponnese in 2019. His master thesis focused on the performance analysis of Spatial Modulation-MIMO systems for several fading scenarios. He is currently a PhD candidate at University of Peloponnese in collaboration with the National Centre for Scientific Research-“Demokritos”. His current research interests are related to the physical layer of wireless communications with focus on statistical modeling of wireless channels.



Fotis I. Lazarakis received his diploma in Physics in 1990, from Department of Physics, Aristotle University of Thessaloniki, Greece, and his Ph.D in Mobile Communications, in 1997, from Department of Physics, National and Kapodistrian University of Athens, Greece, holding at the same time a scholarship from National Center for Scientific Research “Demokritos” (NCSR), Institute of Informatics and Telecommunications (IIT). From 1999 to 2002 he was with Telecommunications Laboratory, National Technical University of Athens, as a senior research

associate. In 2003 he joined NCSR, Institute of Informatics and Telecommunications as a Researcher and since 2013 is a Research Director. He has been involved in a number of national and international projects, acting as a Project Manager to several of those. His research interests include WLANs, 5G and beyond, propagation models and measurements, fading channel characteristics and capacity, diversity techniques, MIMO antennas and systems, radio resource management and performance evaluation of mobile/wireless networks. Dr. Lazarakis has authored or co-authored more than 100 journal and conference papers and he is co-owner of a patent.



Angeliki Alexiou is a professor at the department of Digital Systems, ICT School, University of Piraeus. She received the Diploma in Electrical and Computer Engineering from the National Technical University of Athens in 1994 and the PhD in Electrical Engineering from Imperial College of Science, Technology and Medicine, University of London in 2000. Since May 2009 she has been a faculty member at the Department of Digital Systems, where she conducts research and teaches undergraduate and postgraduate courses in the area

of Broadband Communications and Advanced Wireless Technologies. Prior to this appointment she was with Bell Laboratories, Wireless Research, Lucent Technologies, (later Alcatel-Lucent, now NOKIA), in Swindon, UK, first as a member of technical staff (January 1999-February 2006) and later as a Technical Manager (March 2006-April 2009). Professor Alexiou is a co-recipient of Bell Labs President's Gold Award in 2002 for contributions to Bell Labs Layered Space-Time (BLAST) project and the Central Bell Labs Teamwork Award in 2004 for role model teamwork and technical achievements in the IST FITNESS project. Professor Alexiou is the Chair of the Working Group on Radio Communication Technologies and of the Working Group on High Frequencies Radio Technologies of the Wireless World Research Forum. She is a member of the IEEE and the Technical Chamber of Greece. Her current research interests include radio interface for 5G systems and beyond, MIMO and high frequencies (mmWave and THz wireless) technologies, cooperation, coordination and efficient resource management for Ultra Dense wireless networks and machine-to-machine communications, ‘cell-less’ architectures based on virtualization and extreme resources sharing and machine learning for wireless systems. She is the project coordinator of the H2020 TERRANOVA project (ict-terranova.eu) and the technical manager of H2020 ARIADNE project (ict-ariadne.eu).



Symeon Chatzinotas (S'06–M'09–SM'13) is currently Full Professor / Chief Scientist I and Co-Head of the SIGCOM Research Group at SnT, University of Luxembourg. In the past, he has been a Visiting Professor at the University of Parma, Italy and he was involved in numerous Research and Development projects for the National Center for Scientific Research Demokritos, the Center of Research and Technology Hellas and the Center of Communication Systems Research, University of Surrey. He received the M.Eng. degree in telecommunications

from the Aristotle University of Thessaloniki, Thessaloniki, Greece, in 2003, and the M.Sc. and Ph.D. degrees in electronic engineering from the University of Surrey, Surrey, U.K., in 2006 and 2009, respectively. He was a co-recipient of the 2014 IEEE Distinguished Contributions to Satellite Communications Award, the CROWNCOM 2015 Best Paper Award and the 2018 EURASIC JWCN Best Paper Award. He has (co-)authored more than 400 technical papers in refereed international journals, conferences and scientific books. He is currently in the editorial board of the IEEE Open Journal of Vehicular Technology and the International Journal of Satellite Communications and Networking.